An extended Pal 5 stream in Gaia DR2

Nathaniel Starkman[⋆], Jo Bovy, & Jeremy J. Webb

Department of Astronomy and Astrophysics, University of Toronto, 50 St. George Street, Toronto, Ontario, M5S 3H4, Canada

Accepted XXX. Received YYY; in original form ZZZ

ABSTRACT

We present the results of a detailed search for members of the Pal 5 tidal tail system in Gaia Data Release 2 (DR2). Tidal tails provide a sensitive method for measuring the current and past gravitational potential of their host galaxy as well as for testing predictions for the abundance of dark matter subhalos. The Pal 5 globular cluster and its associated tails are an excellent candidate for such analysis; however, only $\sim 23^{\circ}$ of arc are currently known, with in particular the leading tail much shorter than the trailing. Using Gaia DR2 and its precise astrometry, we extend the known extent of the Pal 5 tail to $\sim 30^{\circ}$, 7 degrees of which are newly detected along the leading arm. The detected leading and trailing arms are symmetric in length and remain near constant width. This detection constrains proposed models in which the Galactic bar truncates Pal 5's leading arm. Follow-up spectroscopic observations are necessary to verify the candidate stream stars are consistent with the known tidal tails. If confirmed, this Pal 5 stream extension opens up new possibilities to constrain the Galactic potential.

Key words: Galaxy: bulge — Galaxy: halo — globular clusters: individual (Palomar 5) — methods: data analysis — Galaxy: kinematics and dynamics

1 INTRODUCTION

The tidal field of a globular cluster's host galaxy plays an important role in its dissolution, with the outer regions being more strongly affected by tides than the inner cluster regions (Renaud 2018). In the approximation of a smooth Galactic mass distribution, the physical boundary of a globular cluster (GC) can be taken to be the surface along which the external tidal field and the cluster's potential are equal (Renaud et al. 2011). The L1 and L2 Lagrange points mark the locations where this surface intersects with the cluster's radial position vector. Through internal processes, like relaxation and binary interactions, and external processes, like tidal heating and shocking, the anisotropic local tidal field results in stars primarily escaping through these Lagrange points (Ross et al. 1997; Fukushige & Heggie 2000). As the cluster dissolves, leading and trailing tidal stellar tails will form in this way and these are typically referred to as "stellar streams".

One of the most useful stellar streams to study is that of the globular cluster Palomar 5 (Pal 5; Odenkirchen et al. 2001). The Pal 5 cluster lies at a sky position of $(\alpha, \delta) \approx (229^{\circ}, -0.11^{\circ})$ and at a distance of $\sim 23\,\mathrm{kpc}$ (Odenkirchen et al. 2003). Pal 5's tidal tails are both thin and long, extending more than 10 kpc in the most sensitive detection so far (Ibata et al. 2017). Observations of the Pal 5 tidal tail over

the years, starting with the first detection by Odenkirchen et al. (2001), who found $\sim 10^{\circ}$ total of tidal tail, has consistently found the trailing arm to be longer than the leading arm. Grillmair & Dionatos (2006) increased the detection limits to about 16° along the trailing arm and 6° along the leading arm using SDSS data (Adelman-McCarthy et al. 2006), but detection of the leading arm was limited by the edge of the SDSS imaging survey footprint. Subsequent studies have reproduced or extended these findings with different datasets. Carlberg et al. (2012) claims an extension of the trailing arm to nearly 23° using SDSS DR8 data. Again, the detection was limited by the survey footprint on the leading edge. Ibata et al. (2016) used Canada French Hawaii Telescope (CFHT) data to recover 19° of stream, mainly along the trailing arm. Finally, Bernard et al. (2016) used Pan-STARRS data to recover the $\sim 22^{\circ}$ of stream from Grillmain & Dionatos (2006), including the truncation of the leading arm at $\sim 8^{\circ}.$ The Pan-STARRS data extends to lower declination than the SDSS data and for the first time, the truncation in the leading arm was considered to be an intrinsic feature of the stream rather than an observational effect. In total, only ~23° have been conclusively detected, despite various attempts. This detection is asymmetric – $\sim 8^{\circ}$ of leading arm, $\sim 15^{\circ}$ of trailing arm – favoring the trailing arm.

From simulations of the formation of the Pal 5 tidal stream, we expect approximately symmetric tails (Dehnen et al. 2004) and the leading arm truncation is therefore puzzling. We furthermore expect the tails to be longer than the observed extent, because the combined mass function of Pal

^{*} E-mail: n.starkman [at] mail.utoronto.ca

5 and its tail has a slope of ~ 0.6 (Grillmair & Dionatos 2006). This value is far from the believed primordial initial mass function, suggesting more stars have been lost than can currently be accounted for. The missing stars should therefore compose an extended and symmetric tidal tail (Koch et al. 2004).

To explain the leading-arm truncation, Pearson et al. (2017) propose that the Galactic bar can induce stream asymmetry for certain values of the bar's pattern speed. They additionally predict the leading arm should reappear further South. However, it remains possible that the asymmetry in the detected tails may be the result of observational limitations: the leading arm more strongly overlaps with the bulge, making its detection more difficult.

A data-set with a footprint and depth that allows one to search beyond previous surveys presents an enormous opportunity to extend the Pal 5 tidal tails and constrain the interaction history of the Pal 5 cluster with the Galaxy. The Gaia Data Release 2 data-set (Gaia DR2; Gaia Collaboration et al. 2018) fulfills the above two requirements. Gaia is an all-sky survey comprising over 1.3 billion stars out to distances exceeding 23.5 kpc (the approximate distance of Pal 5). Moreover, unlike previous surveys, Gaia has parallax and proper motion measurements for most of its stars, which are useful for identifying a spatially and kinematicallycontinuous tidal tail. One drawback of the Gaia data is the photometric uncertainty, which is relatively large compared to other surveys, especially at the magnitudes of detectable Pal 5 stars. However, by cross-matching Gaia DR2 to the Pan-STARRS survey (Chambers et al. 2016), we are able to build a database with kinematics from Gaia DR2 and precise Pan-STARRS photometry that combines the best aspects of both surveys.

The purpose of this study is to use the combined *Gaia* DR2 - Pan-STARRS dataset to search for Pal 5's tidal tails. The outline of this paper is as follows: Section 2 provides details of the data-sets used and the observed properties of the Pal 5 cluster, which form the basis of a set of filters applied in Section 3 to the data-set. These filters allow for stars that are member of the Pal 5 tidal tail to be identified, extending its length far beyond previous detection limits. We summarize the results and their implications in Sections 4 and 5.

2 OBSERVATIONS

The Pal 5 cluster, while undergoing tidal dissolution, is still well-defined (Dehnen et al. 2004) and can be easily identified in Gaia DR2 as an overdensity of points in right ascension and declination (α,δ) . Proper motions and the cluster's locus in the colour-magnitude diagram (CMD) help constrain cluster membership even further. As previously discussed, stars which escape Pal 5 are expected to populate tidal tails that precede and proceed the cluster along its orbit. The following data cuts that reveal the cluster will likewise distinguish the tidal tail.

2.1 Gaia Data

We obtained observational data from a Gaia DR2-Pan-STARRS cross-matched catalogue, available via the Gaia

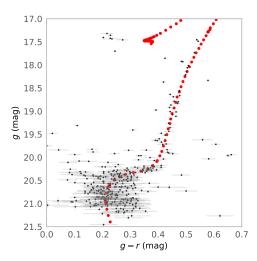


Figure 1. CMD of all stars with $\varpi < 1$ mas within 3 arc-minutes of the center of Pal 5. The locus of Pal 5 is strongly apparent with a well-populated giant branch and MSTO. Though sparse, there is a distinguishable horizontal giant branch and collection of blue stragglers. The latter are not used when constructing the CMD filter.

data portal (Gaia Collaboration et al. 2016; Luri et al. 2018). The code to perform this cross-match and subsequent analysis will be made publicly available 1 . To select stars in the cross-matched catalogue that could be members of the Pal 5 tails, we construct a sky-rotated coordinate system which locally linearizes the Pal 5 tail about a point. The proper sky rotation for Pal 5 cannot be known a priori; hence the sky-rotation matrix is defined by proxy using an N-body simulation of Pal 5 and its tidal tails. We define the Pal 5 cluster-centered system with the coordinates ϕ_1 - - along the direction of the tails—and ϕ_2 —perpendicular to the tail. We select the rotation such that, moving from the cluster, the tails curve up toward positive ϕ_2 . The details of the coordinate system are provided in Appendix B.

2.2 Parallax Cut

The Pal 5 cluster is thought to be approximately 23 kpc away (Odenkirchen et al. 2003; Bovy et al. 2016b). In Gaia DR2, main-sequence turn-off (MSTO) stars can be seen to this distance near Gaia's faint limit, but the data do not have precise parallax measurements in this regime (Gaia Collaboration et al. 2018). Consequently, we only constrain parallaxes ϖ to be less than 1 mas to cut all data closer than 1 kpc. More stringent cuts are too restrictive given the errors. With this cut the Pal 5 GC is clearly present, but the tail is indistinguishable from foreground or background objects. Further selection procedures are needed. Therefore we next examine the Pal 5 GC's proper motion and locus in the colour-magnitude diagram to determine the filters necessary to extract the extended tails.

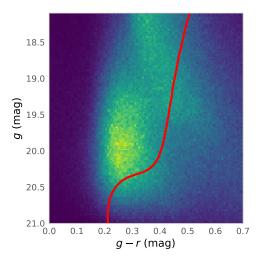


Figure 2. The background distribution of stars in the *Gaia* DR2 data window around the Pal 5 cluster. The bulge is clearly visible in the histogram, coloured by the logarithm of the density. Overlayed on the bulge is the best-fit isochrone. The densest region of the bulge almost directly overlays Pal 5's main sequence turn-off.

2.3 Proper Motion Cut

An advantage of *Gaia* over previous instruments is its ability to accurately measure stellar kinematics. Pre-*Gaia* stream detections have generally been limited to photometry. To remain coherent on the sky, stars in a stellar stream need to be close to co-moving and the kinematics of the tails are similar to that of the progenitor, with differences owing primarily to the tidal dissolution process. As the process can be be modeled (e.g., Kruijssen & Mieske 2009; Bovy 2014; Webb & Bovy 2019; Balbinot & Gieles 2018), examining the cluster's kinematics allows for tail stars to be identified amongst background stars not associated with Pal 5.

The kinematics of the cluster have been measured often, most recently by Vasiliev (2019) using the latest Gaia DR2 data. Our findings agree with Vasiliev (2019): both in right ascension and declination, the proper motion distribution of stars within 2 projected tidal radii of Pal 5 is sharply peaked around -2.7 (mas yr⁻¹). Although this peak suggests individual cluster members may be identified by only their proper motion and spatial clustering, at the distance of Pal 5, the errors in Gaia DR2 proper motion data preclude this direct approach.

As will be explained in Section 3.2 below, in order to isolate the tidal tail, we make a less restrictive proper motion cut by selecting a circle in right ascension and declination proper motion space that encompasses the Pal 5 tails' proper motion distribution and accounts for the significant errors in the proper motions. The proper motion cut allows for the tails' location in the CMD to be identified.

2.4 Colour-Magnitude Cut

Complimentary to the proper-motion strategy to isolate the Pal 5 cluster and tail is a more traditional photometric selec-

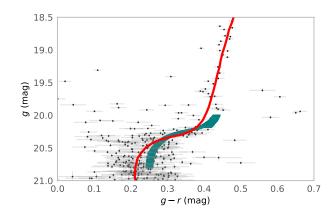


Figure 3. The colour-magnitude cut used to find the extended Pal 5 tidal tails. The black dots are stars with $\varpi < 1$ mas within 3 arc-minutes of the center of Pal 5. An isochrone is fit through the cluster. The CMD cut (teal) is constructed based off this isochrone, and is limited to 20 < g < 20.7 mag.

tion, accomplished using the CMD of the cluster. In Figure 1 the cluster's locus is well defined in the CMD in the g and r Pan-STARRS bands. These bands are optimal for detecting main-sequence stars (the majority of tail stars) and distinguishing tail-stars from foreground and background objects (Ibata et al. 2017). A range of isochrones can be fit to Pal 5's CMD due to the age-metallicity-distance degeneracy in isochrone tracks. As we are not intending to precisely distance or age Pal 5, any isochrone fitting the data is sufficient. We find that a PARSEC isochrone (Bressan et al. 2012) with an age of 11.2 Gyr and metallicity [Fe/H] = -3.072 fits the locus of the Pal 5 stars well². Placed at a distance of \sim 22 kpc, the isochrone tracks the MSTO and the giant branch.

Past work on detecting the Pal 5 tidal tails has always fit a CMD-cut directly to the Pal 5 cluster (see, e.g., Ibata et al. 2016). This works well when using data-sets with deep photometry. However, as is apparent in Figure 1, the main sequence (MS) of Pal 5 is poorly constrained in Gaia DR2, even with Pan-STARRS-crossmatched photometry. This is because it is largely below Gaia's magnitude limit and fainter than a magnitude of ~ 21 , the g-band photometry is noisedominated. The noise is problematic as the majority of stars in both the cluster and tail are MS stars. Excluding these stars leaves little data. As a compounding problem, in Section 3, we demonstrate that the foreground, primarily from the Galactic bulge, dominates the CMD near Pal 5 in the region $18 \lesssim g \lesssim 20.7$ mag, cutting into the expected location of the tails' MSTO. The significant amount of foreground stars precludes the standard application of an isochrone-based cut fit directly to the cluster. A solution to this problem is presented in Section 3.3.

¹ https://github.com/nstarman/Pal-5-in-Gaia-DR2

 $^{^2}$ The isochrone was generated using CMD v3.1 (http://stev.oapd.inaf.it/cgibin/cmd_3.1), with the Pan-STARRS photometry and a Marigo et al. (2008) isochrone track.

3 IDENTIFYING THE EXTENDED STREAM

In this section, we describe how we adapt and apply the techniques used in Section 2 to examine the Pal 5 cluster, to reveal a much-extended length of the Pal 5 tidal tails.

3.1 Parallax and Magnitude Cut

Like in Section 2, we apply a $\varpi < 1$ mas cut to remove nearby stars from the dataset. The photometric depth of the Gaia DR2 - Pan-STARRS cross-match catalogue is approximately $g \sim 21$ for stars with $-0.2 \lesssim g-r \lesssim 0.6$, the range relevant for Pal 5 members. As shown in Figure 1, at the distance of Pal 5 the majority of the main sequence lies below g=21. At $g \gtrsim 20.5$ the data becomes progressively more noise dominated. Because few stars occupy the giant branch of the Pal 5 isochrone, we adopt the g-band filter 20 < g < 20.7. This range encompasses the MSTO and a limited portion of the main sequence, avoiding the noise-dominated measurements nearer $g \sim 21$ mag.

3.2 Proper Motion Cut

While the kinematics of the Pal 5 cluster are fairly well constrained (Vasiliev 2019) and the tidal tail kinematics are similar to that of the cluster, predicting the tails' exact proper motion at distances far from Pal 5 is not trivial. The tidal dissolution process may be modeled (e.g., Webb et al. 2014; Bovy 2014), but it is an area of active research and different models predict different proper motion distributions. Additionally, the choice of Galactic potential model has a large effect on the resulting stream kinematics (Bovy et al. 2016b). We use an N-body simulation, described in Appendix A, to constrain the range of proper motions that tail stars could have.

The proper motion cut is constructed by taking a circle in μ_{α^*} and μ_{δ} near the centroid of the *N*-body simulation's proper motion distribution. The circle center is located at $(\mu_{\alpha^*}, \mu_{\beta}) = (-2.5, -2.5)$ mas yr⁻¹, which better reflects the whole system as opposed to just the GC. The selection radius is 3 mas yr⁻¹ encompasses the data points at the extrema of the tails to around the 1- σ level after accounting for the observational errors.

3.3 Colour-Magnitude Cut

Standard practice to isolate the Pal 5 cluster and its tidal tails is to select stars within some region surrounding Pal 5's locus in the CMD using an isochrone (Grillmair & Dionatos 2006; Ibata et al. 2016). In Section 2.4, we fit an isochrone to the cluster's CMD locus that could serve as the basis of such a filter. However, the standard isochrone approach fails due to the dominance of the Galactic bulge, whose stars overlap with and far outnumber the stars in Pal 5's MSTO. For deep photometric surveys, such as used in the two aforementioned papers, the CMD cut extends into Pal 5's main sequence where there is little contamination from the bulge. However, at the brighter magnitudes accessible in Gaia, a significant population of Galactic bulge stars exists in a similar part of the CMD as Pal 5's MSTO region. A standard CMD cut around the best-fit isochrone therefore does not reveal the extended Pal 5 tails as it picks up too many bulge

foreground stars. The dominance of the bulge may be seen in Figure 2. Overlayed on the plot is the best-fit isochrone (Section 2.4). The bulge distribution is most dense around $(g-r,g)\sim(.25,20.2)$, abutting the top of the cluster's MSTO, where nearly all Gaia-observable stars live.

Without an extended MS, the presence of the bulge precludes the standard isochrone approach. The solution is to construct a CMD cut as far away as possible from the Galactic bulge locus, while still maintaining enough Pal 5 stars to observe the tails. Figure 3 demonstrates this careful balancing act. The red line is the isochrone described in Section 2.4 (with an age of 11.2 Gyr and a metallicity of [Fe/H] = -3.072). This is the isochrone about which a standard CMD cut would be constructed. The width of the CMD cut would be set by the stellar overdensity and be thinnest at the MSTO. Instead, the CMD shown in teal is used. This 'shifted'-CMD is the region between two translations of the best-fit isochrone in colour-magnitude space, with an additional broadened region on the giant branch of the Pal 5 isochrone. The translation distance of the 'shifted'-CMD from the best-fit isochrone is selected such that the bulge locus is avoided, while the majority of the MSTO remains within the selection. A CMD shifted further than this contains insufficient cluster and tails stars, while much closer CMDs fall prey to the Galactic bulge. The upper region of the 'shifted'-CMD is manually broadened to track the stars with $\varpi < 1$ mas within 3 arc-minutes of the center of Pal 5. These stars, shown in Figure 3, do not appear to lie along the best-fit isochrone, necessitate the broadened selection in this region.

While the Pal 5 tail has a distance gradient, the background does not. Also, at ~23 kpc, the colour-magnitude locus of the Galactic bulge lies at lower magnitude than the cluster isochrone. Since the Pal 5 cluster is near apocenter at the other side of the Galaxy relative to us, the leading and trailing tails lie closer than the cluster and thus move progressively into the Galactic bulge's locus in the CMD the further along the tail one travels. Nearer regions of the tidal tails have even stronger overlap than the cluster to the Galactic bulge. However, as the tail shifts to lower gmagnitude it brings stars in the tails' MS above Gaia's magnitude limit. Therefore, disregarding the distance gradient and keeping the CMD cut static allows the true CMD along the tail to sweep through the CMD cut as defined around the cluster, and minimize the number of Galactic bulge stars selected by this cut.

3.4 Smoothing Kernel

To maximize the signal-to-noise of the tails star-count overdensities, we use a Gaussian smoothing kernel of $\sim 0.1^{\circ}$, approximately the same angular width as the tails. We motivate the smoothing width by examining the previouslydetected tail lengths, such as those in Ibata et al. (2016) and Grillmair & Dionatos (2006). This single-kernel approach has two drawbacks. First, the characteristic width of the Pal 5 tails is not precisely determined. Both internal and external kinematics of the cluster are important to the tail width, as well as the precise potential of the Galaxy and the interaction history of Pal 5 with its environment. Second, Nbody simulations of Pal 5, such as from Section A, predict a spatial broadening along the tail. Therefore, there is no sin-

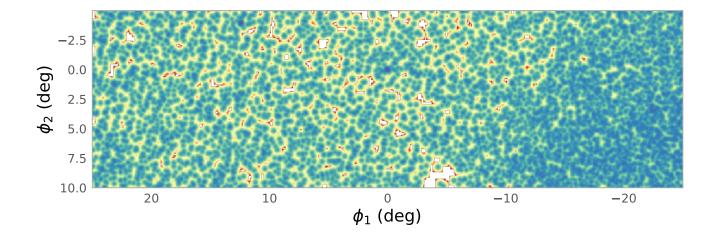
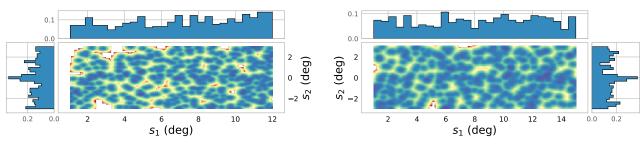


Figure 4. The Pal 5 data-set with all cuts— parallax, proper motion, colour-magnitude, Gaussian filter—applied. The leading and trailing arms clearly extend from the progenitor at $(\phi_1, \phi_2) = (0, 0)$ for $\sim 15^{\circ}$ on both sides. The leading arm becomes indistinguishable past $\sim (15, 2.5)^{\circ}$, while the trailing arm does so at $\sim (-12, 2.5)^{\circ}$.



- (a) Sky projection onto an orbit fit to the trailing arm
- (b) Sky projection onto an orbit fit to the leading arm

Figure 5. These figures show the nearest 3° of the Pal 5 data-set projected along orbits fit to the tails. The coordinate s_1 tracks the tail arc-length, and s_2 is the orthogonal distance from the tails, which are centered on $s_2 = 0$. The left plot displays the leading arm of the Pal 5 tidal tail, starting a distance of 1° from the cluster so as not to include any cluster stars. The tail is visible for ~15°. The right plot is that of the trailing arm. On this side the tail is visible for at least 12°.

gle characteristic tail spatial width. However, as predicted by the N-body simulation, the tail remains thin for tens of degrees on either side of the cluster. Also, because we aim to measure the tails' length and not their detailed properties, small deviations from a single width are not important. For these reasons, despite theoretical drawbacks, the single-kernel approximation remains valid along the tails' detected length.

3.5 Dust Foregrounds and Observational Cadence

We examine the data-set to ensure dust foregrounds and Gaia's observational cadence are not mistaken for the tidal tail. Photometric dust extinctions in the Pan-STARRS g and r are obtained using the mwdust package (Bovy et al. 2016a). Examining the dust maps reveals no structure in the dust to which the detected tail might be attributed. Likewise, a hexagonal tiling pattern from Pan-STARRS, observable in some proper motion cuts, is not consistent with the tidal tail. We also note that vertical striping from Gaia's observational cadence is nearly orthogonal to the tail and cannot explain the observation. Finally, no systematic discussed in

Gaia Collaboration et al. (2018) aligns with the predicted (or past measured) tail path within at least 20 degrees of the cluster. Therefore, the observed tidal tail is not a dust or observation-strategy artifact—indicating it is a true measurement.

4 RESULTS

Applying the filters and processing from Section 3 reveals Pal 5's tidal tails in Figure 4. On the trailing arm—in the negative ϕ_1 direction—the arm becomes indistinguishable from background after ~12°. On the opposite side, the leading arm extends ~15°, though there are hints it goes further (see Figure 4), before likewise becoming indistinct. Overall, this represents a ~27° detection of the Pal 5 tidal tail and an extension of the leading arm by ~7°.

Prior detections of Pal 5's tidal tail have mostly been along the trailing arm, starting from Odenkirchen et al. (2003) to Bernard et al. (2016), as described in Section 1. In total, only $\sim 8^\circ$ has been detected along the leading arm, while we recover 15°. Along the trailing arm, we find the stream along 12°, only slightly shorter than prior detections,

Table 1. Positions and velocities for the orbits hand-fit to the sky positions of the tidal tails for the purpose of straightening the tails. Projections of stars within 3 ° of these orbits are shown in Figure 5.

arm	$\alpha, \delta(^{\circ})$	d(kpc)	$\mu_{\alpha^*}, \mu_{\delta} (\text{mas yr}^{-1})$	$v_r (\text{km s}^{-1})$
Leading	229.022, -0.223		-2.16, -2.23	-40
Trailing	229.022, -0.223		-2.00, -2.18	-50

which detect the trailing arm out to $\sim 15^{\circ}$ (Bernard et al. 2016). The total length of the Pal 5 stream is therefore $\sim 30^{\circ}$, symmetric around the progenitor.

While many of the prior studies have deeper photometry than is available in *Gaia* DR2, none have as extensive kinematic nor parallax data. These data have proved a crucial development to stream searches. Stream-search algorithms, such as developed by Malhan & Ibata (2018) and Palau & Miralda-Escudé (2019), have discovered many new streams too faint to detect using purely photometric techniques. It is in this same vein that we present extensions to the Pal 5 tidal tail. *Gaia* DR2 photometry is not deep, but the extensive astrometric data permits more restrictive phase-space reductions than in prior data sets, and when combined with photometric and parallax restrictions, reveals an extended Pal 5 tidal tail.

All the phase-space restrictions described in Section 3 are necessary to identify the Pal 5 tidal tails. The 1 kpc parallax filter removes the majority of foreground objects. The proper motion filter removes 81% of the remaining stars, most importantly objects such as the large M5 globular cluster, which lies within 2 degrees of the Pal 5 cluster. The single most restrictive cut is that of the shifted-CMD, motivated in Section 3.3. This CMD cut removes 98 % of the remaining stars in the selected Gaia window. While many potential tail stars are cut, the CMD cut crucially removes most foreground objects, particularly the bulge stars which enshroud the tidal tail. The CMD cut is particularly efficacious along the Pal 5 leading arm and permits a 15° tail-length detection.

Corroborating the visual detection of the tail are the projections of the Gaia DR2 data on orbits hand-fit to align with the observed tidal tails. These projections are shown in Figure 5 for both the leading and trailing arms. The orbits are only fit to the tail in α and δ and are not predictions of the actual orbital dynamics of the tidal tail; we only use them to provide a convenient parametrization of the path of the tails. The positions and velocities of these hand-fit orbits are given in Table 1. Stars within 3° of the orbits are selected and represented in the on-stream coordinate system (s_1, s_2) —the arc length along and orthogonal distance to the stream, respectively. The fits along s_2 confirm an enhancement at $s_2 = 0$, the location of the tails, above the background level of the star count near the tails.

We compute the significance of our new detection using Poisson anomaly detection on the binned star counts. As the stream is spread over multiple bins, we calculate the likelihood of observing a set S stream-bins, from n bins total, with star counts f and median \bar{x} as

$$p = (n-2) \prod_{i \in S} (1 - \text{CDF}_{\text{Poisson}}(\mathbf{f}_i, \bar{\mathbf{x}})).$$

S is the index set for bins in the stream, with number of elements $\geq s$. The (n-2) factor accounts for the fact that

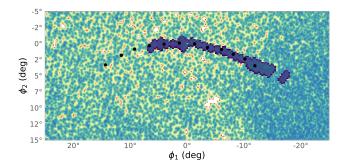


Figure 6. Comparison between our Pal 5 stream detection and previous work. We overplot the Ibata et al. (2016) data on the Gaia DR2 data-set of this paper. Also shown are a number of black points which are placed along our observed tails to assist in comparing the two data-sets. Over the region where the data-sets overlap, the tidal tails agree.

the anomaly could have been detected in any of the bins, except for the edge bins. Figure 5 shows a 3 degree region surrounding each stream. The leading arm and trailing arms have at least 2 stream bins, corresponding to a width of $\sim 0.5^\circ$ and consistent with previous studies (e.g., Grillmair & Dionatos 2006). Using the data cuts previously described, from these bins, we achieve a > 3 σ detection along each the trailing and leading arms. The significance of the newly-detected part of the leading arm, excluding the previously detected 8° , is also $\geq 3\,\sigma$.

An important validation of our approach is that of consistency with prior work. The dataset used in Ibata et al. (2016) is publicly available on the VizieR database. Figure 6 shows that the observed tidal tail exactly tracks with the results of Ibata et al. (2016). We also checked against the results of Carlberg et al. (2012) and find consistent results.

5 CONCLUSIONS

To date, $\sim 23^{\circ}$ of Pal 5's tidal tails have been detected, with the leading arm significantly shorter than the trailing arm (Bernard et al. 2016). As explained in Section 1, we expect longer and more symmetric tidal tails unless the Pal 5 stream has been significantly perturbed.

There is a convergence of factors which make the Pal 5 tidal tail difficult to detect in Gaia DR2. First, it is distant, requiring deeper photometry than is available in Gaia DR2. Second, at this distance, the proper motions in Gaia DR2 have fractional errors of order unity. Third, the Galactic bulge overlays part of Pal 5's MSTO, the highest numberdensity area available in the CMD. However, using a parallax, proper motion, and CMD cut, and applying Gaussian spatial smoothing, we report a detection of ~27° of Pal 5's tidal tails. Of this, $\sim 7^{\circ}$ are newly-detected extensions to the Pal 5 tails. Combined with previous detections of the trailing tail, we find a total length of $\sim 30^{\circ}$, 15° on each side of the Pal 5 cluster. Given the distance to Pal 5, stars populating the region of the tail $\sim 15^{\circ}$ away escaped the cluster several Gyr ago (Dehnen et al. 2004). Given the length and width of the tail, the cluster has been continuously losing mass for several Gyr without a major disruption event.

Most importantly, the extension we find lies entirely along the leading arm, which has historically been found to be significantly shorter than the trailing arm (Odenkirchen et al. 2001). Taking our newly-detected extension into account, the two arms are roughly equal in length. This is in contrast to previous studies, many of which speculate that the leading arm is truncated compared with the trailing arm. Pearson et al. (2017) hypothesize that interactions with the bar curtail (or prevent) stars escaping into the leading arm and thus cause an underdensity (or gap) in the leading arm, starting at ~8°. Our finding of symmetric tidal tails constrains this scenario. As we are sample limited, we cannot rule out scenarios which reproduce our threshold density past ~8°. Thus, we do not eliminate models with any barstream interactions. However, the presence of symmetric and continuous arms precludes models in which true gaps form from interactions with the bar.

The extended tails can improve constraints on the Galactic potential. In particular, the tails are sensitive to the shape of the Galactic halo (Bovy et al. 2016b; Pearson et al. 2015) and longer tails are more constraining. Banik & Bovy (2019) suggest that Pal 5 is a poor candidate for dark matter subhalo searches. However, the extended tidal tails will afford the opportunity to search for overdensities characteristic of epicycle bunching Küpper et al. (2012) and barinduced underdensities. Follow-up observations are needed to confirm the potential tail stars are chemically and kinematically compatible with the cluster.

ACKNOWLEDGMENTS

JB and JJW received support from the Natural Sciences and Engineering Research Council of Canada (NSERC; funding reference number RGPIN-2015-05235) and from an Ontario Early Researcher Award (ER16-12-061).

This work presents results from the European Space Agency (ESA) space mission Gaia. Gaia data are being processed by the Gaia Data Processing and Analysis Consortium (DPAC). Funding for the DPAC is provided by national institutions, in particular the institutions participating in the Gaia MultiLateral Agreement (MLA). The Gaia mission website is https://www.cosmos.esa.int/gaia. The Gaia archive website is https://archives.esac.esa.int/gaia.

REFERENCES

```
Aarseth S., 2006, Gravitational N-Body simulations. Vol. 38, Cambridge University Press, doi:10.1007/s10714-006-0278-1
Adelman-McCarthy J. K., et al., 2006, ApJS, 162, 38
Balbinot E., Gieles M., 2018, MNRAS, 474, 2479
Banik N., Bovy J., 2019, MNRAS, 484, 2009
Bernard E. J., et al., 2016, MNRAS, 463, 1759
Bovy J., 2014, ApJ, 795, 95
Bovy J., 2015, ApJS, 216, 29
Bovy J., Rix H.-W., Green G. M., Schlafly E. F., Finkbeiner D. P., 2016a, ApJ, 818, 130
Bovy J., Bahmanyar A., Fritz T. K., Kallivayalil N., 2016b, ApJ, 833, 31
Bressan A., Marigo P., Girardi L., Salasnich B., Dal Cero C., Rubele S., Nanni A., 2012, MNRAS, 427, 127
```

Carlberg R. G., Grillmair C. J., Hetherington N., 2012, ApJ, 760,

```
Chambers K. C., et al., 2016, arXiv e-prints, p. arXiv:1612.05560
Dehnen W., Odenkirchen M., Grebel E. K., Rix H.-W., 2004, AJ,
   127, 2753
Fukushige T., Heggie D. C., 2000, MNRAS, 318, 753
Gaia Collaboration et al., 2016, A&A, 595, A1
Gaia Collaboration et al., 2018, A&A, 616, A1
Grillmair C. J., Dionatos O., 2006, ApJ, 641, L37
Grillmair C. J., Smith G. H., 2001, AJ, 122, 3231
Hurley J. R., Pols O. R., Tout C. A., 2000, MNRAS, 315, 543
Hurley J. R., Tout C. A., Pols O. R., 2002, MNRAS, 329, 897
Ibata R. A., Lewis G. F., Martin N. F., 2016, ApJ, 819, 1
Ibata R. A., Lewis G. F., Thomas G., Martin N. F., Chapman S.,
   2017, ApJ, 842, 120
Ibata R. A., Bellazzini M., Malhan K., Martin N., Bianchini P.,
   2019, Nature Astronomy, p. 258
Koch A., Odenkirchen M., Grebel E. K., Martínez-Delgado D.,
   Caldwell J. A. R., 2004, in Prada F., Martinez Delgado D.,
   Mahoney T. J., eds, Astronomical Society of the Pacific Con-
   ference Series Vol. 327, Satellites and Tidal Streams. p. 333
   (arXiv:astro-ph/0307496)
Kroupa P., 2001, MNRAS, 322, 231
Kruijssen J. M. D., Mieske S., 2009, A&A, 500, 785
Küpper A. H. W., Lane R. R., Heggie D. C., 2012, MNRAS, 420,
   2700
Luri X., et al., 2018, A&A, 616, A9
Malhan K., Ibata R. A., 2018, MNRAS, 477, 4063
Marigo P., Girardi L., Bressan A., Groenewegen M. A. T., Silva
   L., Granato G. L., 2008, A&A, 482, 883
Miyamoto M., Nagai R., 1975, PASJ, 27, 533
Navarro J. F., Frenk C. S., White S. D. M., 1996, ApJ, 462, 563
Odenkirchen M., et al., 2001, ApJ, 548, L165
Odenkirchen M., et al., 2003, AJ, 126, 2385
Palau C. G., Miralda-Escudé J., 2019, arXiv e-prints, p.
   arXiv:1905.01193
Pearson S., Küpper A. H. W., Johnston K. V., Price-Whelan
   A. M., 2015, ApJ, 799, 28
Pearson S., Price-Whelan A. M., Johnston K. V., 2017, Nature
   Astronomy, 1, 633
Renaud F., 2018, New Astron. Rev., 81, 1
Renaud F., Gieles M., Boily C. M., 2011, MNRAS, 418, 759
Ross D. J., Mennim A., Heggie D. C., 1997, MNRAS, 284, 811
Vasiliev E., 2019, MNRAS, 484, 2832
Webb J. J., Bovy J., 2019, MNRAS, 485, 5929
```

APPENDIX A: THE N-BODY SIMULATION

MNRAS, 442, 1569

Webb J. J., Leigh N., Sills A., Harris W. E., Hurley J. R., 2014,

We use an N-body simulation of Pal 5 to inform the tidal tail search. The N-Body simulation uses the the direct N-body code NB0DY6 (Aarseth 2006) to simulate the evolution of a Pal 5-like globular cluster. The initial cluster is taken to be a Plummer model consisting of 100,000 stars and has a half-mass radius of 10 pc. Stellar masses follow a Kroupa initial mass function (Kroupa 2001), with the minimum and maximum stellar mass set to $0.1M_{\odot}$ and $50M_{\odot}$ respectively. Single stars evolve using the stellar evolution prescription of Hurley et al. (2000) assuming a metallicity of Z=0.001 while binary stars, in the event that binaries form, follow Hurley et al. (2002).

The properties of the external tidal field were set to reflect MwPotential2014, from Bovy (2015), and is a good approximation of the Galactic potential (Bovy et al. 2016b). The specific linear combination of potentials is a spherical

8 Starkman, Bovy, & Webb

potential from a power-law density with an exponential cutoff Galactic bulge, an NFW dark matter halo (Navarro et al. 1996), and a Miyamoto & Nagai (1975) disc. The model cluster was evolved for 12 Gyr with an initial position and velocity that resulted in it being located at the present day location of Pal 5 at the end of the simulation. The final mass and mass function of the model cluster are comparable to the observed properties of Pal 5 (Ibata et al. 2017; Grillmair & Smith 2001), but the model cluster is too compact relative to Pal 5, which is in the process of dissolving. Changes in the internal dynamics can manifest as differences in the proper motion of tidal tail stars (Ibata et al. 2019); however, small deviations of the potential model to the actual Galactic potential have a more pronounced effect. As the simulation is primarily used to constrain the kinematics of escaped stars (not the cluster's properties at formation), it was not necessary to reproduce Pal 5 itself exactly.

APPENDIX B: CONSTRUCTING THE COORDINATE SYSTEM

To locally-linearize the Pal 5 tidal tail about the cluster we construct an ICRS sky-rotated coordinate system, with onsky angles ϕ_1 and ϕ_2 . It is constructed as follows: first, select a point along the path of the *N*-body simulation as the origin; second, using the path of the *N*-body simulation, rotate and translate the coordinate system until the leading arm is oriented along the positive ϕ_1 axis. We found the Cartesian rotation matrix from ICRS to sky-rotated coordinates to be:

$$\begin{bmatrix} -0.656 & -0.755 & -0.002 \\ -0.537 & 0.468 & -0.701 \\ 0.530 & -0.459 & -0.713 \end{bmatrix}$$
 (B1)

This rotation places the origin at the cluster and Pole of this coordinate system at $(\alpha_{ngp}, \delta_{ngp}) = (319.27^{\circ}, -48.31^{\circ})$. In this sky rotation, the on-tail angle is ϕ_1 and the orthogonal angle is ϕ_2 . For the data window, we select a $|\phi_1| < 10^{\circ}$ by $|\phi_2| < 5^{\circ}$ data window centered on the Palomar 5 cluster as well points along the *N*-body simulation. The data is stitched together to form a continuous window along the *N*-body simulation's path. The selected data window gives a large length of tidal tail, as well as background, to study.

APPENDIX C: QUERYING GAIA DATABASE

Queries to the *Gaia* database are done in ADQL. We provide here the query used to retrieve a dataset containing Pal 5 and a large area of background. The size of the dataset exceeds the download limit of the *Gaia* database and must be performed on a local version of the data, as described in the gaia_tools package. This query was constructed using the make_query function of that package.

```
SELECT
                                                                   gaia.source_id,
gaia.source_id AS id,
                                                                   gaia.parallax, gaia.parallax_error,
gaia.parallax AS prlx, gaia.parallax_error AS prlx_err,
                                                                   gaia.ra, gaia.ra_error,
gaia.ra, gaia.ra_error AS ra_err,
                                                                   gaia.dec, gaia.dec_error,
gaia.dec, gaia.dec_error AS dec_err,
                                                                   gaia.pmra, gaia.pmra_error,
gaia.pmra, gaia.pmra_error AS pmra_err,
                                                                   gaia.pmdec, gaia.pmdec_error,
gaia.pmdec, gaia.pmdec_error AS pmdec_err,
                                                                  -0.6558*cos(radians(dec))*cos(radians(ra))+
ps1.g_mean_psf_mag AS g, ps1.g_mean_psf_mag_error AS
                                                                   -0.7549*cos(radians(dec))*sin(radians(ra))+

    g_err,

                                                                   -0.0022*sin(radians(dec)) AS cosphi1cosphi2,
ps1.r_mean_psf_mag AS r, ps1.r_mean_psf_mag_error AS
     → r_err,
gaia.phi1, gaia.phi2, gaia.pmphi1, gaia.pmphi2
                                                                   -0.5373*cos(radians(dec))*cos(radians(ra))+
                                                                   0.4688*cos(radians(dec))*sin(radians(ra))+
FROM (
                                                                   -0.7011*sin(radians(dec)) AS sinphi1cosphi2,
   SELECT
   gaia.source_id,
                                                                   0.5303*cos(radians(dec))*cos(radians(ra))+
                                                                   -0.4586*cos(radians(dec))*sin(radians(ra))+
   gaia.parallax, gaia.parallax_error,
                                                                   -0.7131*sin(radians(dec)) AS sinphi2,
   gaia.ra, gaia.ra_error,
   gaia.dec, gaia.dec_error,
   gaia.pmra, gaia.pmra_error,
                                                                   -0.9243*cos(radians(dec))-
   gaia.pmdec, gaia.pmdec_error,
                                                                   0.3817*sin(radians(dec))*cos(radians(ra-
                                                                   342.0008)) as c1,
   gaia.sinphi1cosphi2, gaia.cosphi1cosphi2,

→ gaia.sinphi2,

                                                                   0.3817*sin(radians(ra-342.0008)) as c2
   gaia.phi1, gaia.phi2, gaia.c1, gaia.c2,
   ( c1*pmra+c2*pmdec)/cos(phi2) AS pmphi1,
                                                                   FROM gaiadr2.gaia_source AS gaia
   (-c2*pmra+c1*pmdec)/cos(phi2) AS pmphi2
                                                               ) AS gaia
                                                            ) AS gaia
                                                        ) AS gaia
   FROM (
       SELECT
                                                        --Comparing to Pan-STARRS1
       gaia.source_id,
       gaia.parallax, gaia.parallax_error,
                                                        INNER JOIN gaiadr2.panstarrs1_best_neighbour AS
       gaia.ra, gaia.ra_error,

→ panstarrs1_match ON panstarrs1_match.source_id
                                                             gaia.dec, gaia.dec_error,
                                                        INNER JOIN gaiadr2.panstarrs1_original_valid AS ps1 ON
       gaia.pmra, gaia.pmra_error,
       gaia.pmdec, gaia.pmdec_error,
                                                             → ps1.obj_id =

→ panstarrs1_match.original_ext_source_id
       gaia.cosphi1cosphi2, gaia.sinphi1cosphi2,

    gaia.sinphi2,

       gaia.c1, gaia.c2,
                                                        WHERE
                                                            phi1 > -0.4363
       atan2(sinphi1cosphi2, cosphi1cosphi2) AS phi1,
                                                        AND phi1 < +0.4363
       atan2(sinphi2, sinphi1cosphi2 /
                                                        AND phi2 > -0.1745
            AND phi2 < +0.3491

    cosphi1cosphi2))) AS phi2

                                                        AND prlx < 1
       FROM (
                                                        ORDER BY
          SELECT
                                                        gaia.source_id
```